Available online at www.sciencedirect.com
SCIENCE DIRECT®
PERGAMON
International Journal of Heat and Mass Transfer 46 (2003) 4587–4594
International Journal of HEAT and MASS TRANSFER
www.elsevier.com/locate/ijhmt

Flow and heat transfer characteristics of the evaporating extended meniscus in a micro-capillary channel

Kyoungwoo Park [a,1], Kwan-Soo Lee [b,*]

[a] The Center of Innovation Design Optimization Technology, Hanyang University, HIT # 312, 17 Haengdang-dong, Sungdong-gu, Seoul 133-791, South Korea

[b] School of Mechanical Engineering, Hanyang University, 17 Haengdang-dong, Sungdong-gu, Seoul 133-791, South Korea

Received 28 March 2003; received in revised form 7 June 2003

Abstract

A mathematical model is developed to predict the transport phenomena during evaporation in the extended meniscus region of a micro-capillary channel. In this model, the vapor pressure variation and the disjoining pressure effect are included and the friction force at the liquid–vapor interface is considered as well. The results show that the local heat transfer coefficient has an extremely large value in the thin film region. The heat transfer rate, however, is larger for the meniscus than for the thin film region. The maximum liquid velocity appears at approximately 40% of the extended meniscus region and the variation of the heat flux has a negligible effect on the maximum liquid velocity. It is also found that the length of the extended meniscus region is affected by the heat flux, the channel height and the dispersion constant.

Keywords: Micro-capillary channel; Evaporation; Extended meniscus region; Phase change; Control volume

1. Introduction

Due to the miniaturization of the electronic devices resulting from advancements in packaging technology, the heat generated per unit area has dramatically increased. Therefore, the control of the heat generated in micro-scale electronic devices has become an important topic in heat transfer research. A capillary pumped loop (CPL) system has drawn a great deal of attention to the fields of chip-level cooling in micro-scale devices. The CPL system generally consists of an evaporator, condenser, and liquid and vapor lines. The evaporator is the key component of CPL system. It is divided into the meniscus, thin film, and adsorbed regions during the evaporating process of the working fluid. In the thin film region of the evaporator, the heat flux is dramatically increased and therefore, particular efforts have been made to elucidate fundamental heat transfer mechanism in such a micro-scale zone.

Since Derjaguin et al. [1] first analyzed the thermo-fluid characteristics in the evaporating thin film region, a number of excellent numerical and experimental investigations [2–4] have been conducted to predict the flow and thermal characteristics for various evaporator specifications. Recent research on the CPL system has focused on the meniscus region as well as the thin film region. DasGupta et al. [5] studied the transport processes occurring in an evaporating extended meniscus. They suggested the augmented Young–Laplace equation with Kelvin–Clapeyron equation and kinetic theory that can be used to model fluid flow and evaporative heat transfer in the contact line region. Longtin et al. [6] proposed a mathematical model using the control volume method to predict the fluid–thermal characteristics of the micro-heat pipe having a triangular cross section. The effect of disjoining pressure was not included in this model and the liquid and vapor phases were assumed to

* Corresponding author. Tel.: +82-2-2290-0426; fax: +82-2-2295-9021.

E-mail addresses: kwoopark@hanyang.ac.kr (K. Park), ksleehy@hanyang.ac.kr (K.-S. Lee).

[1] Tel.: +82-2-2290-1639.

0017-9310/$ - see front matter © 2003 Elsevier Ltd. All rights reserved.
doi:10.1016/S0017-9310(03)00306-5

Nomenclature

A	area per unit width, m
$\overline{A}$	dispersion constant, J
f	friction coefficient
h	local heat transfer coefficient, W/mK
$\bar{h}$	average heat transfer coefficient, W/mK
h_{fg}	latent heat of vaporization, J/kg
H	channel height, m
K	curvature, m^{-1}
L	length, m
$\dot{m}$	mass flow rate, kg/s
P	pressure, Pa
ΔP	pressure drop, $P_{v,0} - P$, Pa
q''	heat flux, W/m^2
Re	Reynolds number
u, v	velocities of x- and y-direction, m/s
x, y	axial and vertical coordinate, m

Greek symbols

δ	film thickness, m
ρ	density, kg/m^3
μ	viscosity, N s/m^2
v	kinetic viscosity, m^2/s
σ	surface tension, N/m
τ	shear stress, N/m^2

Subscripts

0	inlet or initial
c	capillary
d	disjoining
ev	evaporating
i	liquid–vapor interface
l	liquid
thin	thin film
v	vapor
w	wall

flow in a counter-flow manner. They concluded that the radius of curvature increases linearly along the flow direction. Sartre et al. [7] presented a three-dimensional model for predicting the heat transfer characteristics in the extended meniscus region of a micro-heat pipe array. This model adopted a similar mathematical concept suggested by Longtin et al. and considered the heat conduction effect at the substrate. They reported that both the apparent contact angle and the heat transfer rate increase with increasing wall superheat. Their results, however, are limited to those of the thin film region only. Peles and Harber [8] developed a one-dimensional model that accounts for the boiling two-phase flow and heat transfer phenomena in a triangular micro-channel. They assumed that the vapor pressure was constant and they did not take into account the friction forces both at the liquid–vapor interface and at the solid wall. Qu et al. [9] proposed the mathematical model to account for the formation of evaporating thin liquid film and meniscus in capillary tubes. They investigated the effects of radius and heat transfer on the profile of evaporating extended meniscus region. As mentioned earlier, many studies have assumed a constant vapor pressure and they have not considered the simultaneous effects of the disjoining pressure and the variation in vapor pressure in obtaining the mathematical model in the extended meniscus region.

In this work, a comprehensive mathematical model is presented to describe the two-phase transport phenomena of the extended meniscus region in a micro-capillary channel. The effects of the vapor and disjoining pressures are included in this model. The governing equations are obtained by applying different physical approaches to the meniscus and thin film regions. The effects of the applied heat flux and the inlet liquid velocity on the transport phenomena are investigated. The emphasis is also focused on the effects of the dispersion constant, the channel height, and the heat flux on the location of dry-out point.

2. Mathematical modeling

A working fluid in a micro-capillary channel evaporates due to the applied heat, resulting in the thinner liquid film thickness and an increase in the radius of curvature at the liquid–vapor interface. The phase change phenomenon of a micro-capillary channel of a micro-evaporator is schematically shown in Fig. 1. Heat is applied to both the bottom and top walls of the channel. Only the lower half of a micro-channel is considered due to the geometric symmetry. In this study, the following assumptions are employed to obtain the model:

(1) laminar, incompressible and steady-state for both liquid and vapor flows;
(2) constant properties including the surface tension, and;
(3) negligibly small convective terms in the momentum equation.

The behavior of the liquid–vapor interface is governed by the pressure difference in the liquid and vapor phases. The pressure difference can be expressed by the augmented Young–Laplace equation, which is given by

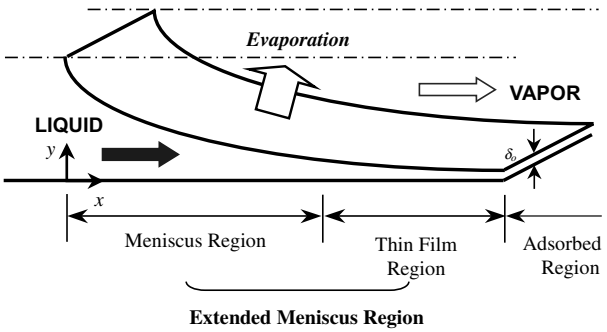

Fig. 1. Schematic diagram of micro-evaporator and its coordinate system.

the summation of the capillary pressure and the disjoining pressure:

$$P_{\mathrm{v}} - P_{\mathrm{l}} = P_{\mathrm{d}} + P_{\mathrm{c}} = -\frac{\overline{A}}{\delta^3} + \sigma K, \tag{1}$$

where δ is the liquid film thickness, $\overline{A}$ the dispersion constant ($=-2.87\times10^{-21}$ J, water), and σ the surface tension. The mean curvature at the liquid–vapor interface (K) can be given as the sum of the x- and z-directional curvatures:

$$K = K_x + K_z = \frac{\mathrm{d}^2\delta}{\mathrm{d}x^2}\left[1+\left(\frac{\mathrm{d}\delta}{\mathrm{d}x}\right)^2\right]^{-1.5} + \frac{1}{(H/2-\delta)}\left[1+\left(\frac{\mathrm{d}\delta}{\mathrm{d}x}\right)^2\right]^{-0.5}, \tag{2}$$

where z-direction is perpendicular to the xy-plane. Substituting Eq. (2) into Eq. (1) and assuming the constant surface tension, the governing equation for the film thickness can be obtained as

$$\frac{\mathrm{d}^2\delta}{\mathrm{d}x^2} + \frac{1}{(H/2-\delta)}\left[1+\left(\frac{\mathrm{d}\delta}{\mathrm{d}x}\right)^2\right] - \frac{1}{\sigma}\left(P_{\mathrm{v}} - P_{\mathrm{l}} + \frac{\overline{A}}{\delta^3}\right) \times \left[1+\left(\frac{\mathrm{d}\delta}{\mathrm{d}x}\right)^2\right]^{1.5} = 0. \tag{3}$$

The profile of the liquid film thickness can be computed using the liquid and vapor pressures as shown in Eq. (3). Therefore, the flow and thermal analyses should be performed in the extended meniscus region.

2.1. Liquid phase

Meniscus region: The theory of momentum over the control volume per unit width (see Fig. 2) is applied for obtaining the mathematical model for the meniscus region. The momentum equation can be written as

$$(\rho_{\mathrm{l}}u_{\mathrm{l}}^2 + P_{\mathrm{l}})\frac{\mathrm{d}\delta}{\mathrm{d}x} + 2\rho_{\mathrm{l}}\delta u_{\mathrm{l}}\frac{\mathrm{d}u_{\mathrm{l}}}{\mathrm{d}x} + \delta\frac{\mathrm{d}P_{\mathrm{l}}}{\mathrm{d}x} = \tau_{\mathrm{l,i}} - \tau_{\mathrm{l,w}}, \tag{4}$$

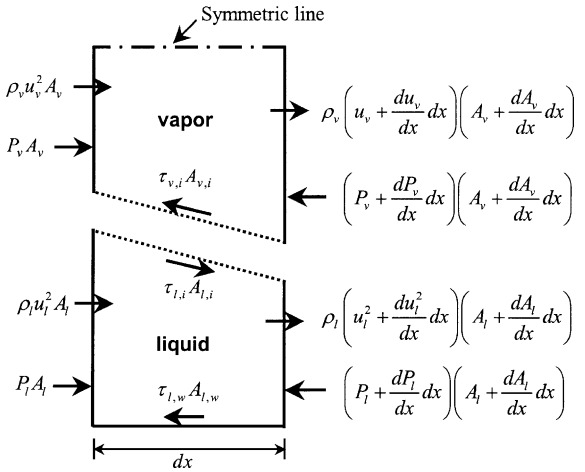

Fig. 2. Momentum equations for liquid and vapor phases in the meniscus region.

where u and τ represent the velocity and shear stress, respectively. In Eq. (4), the shear stresses at the wall and at the liquid–vapor interface are given by [10]

$$\tau_{\mathrm{l,w}} = \frac{1}{2}\rho u_{\mathrm{l}}^2 f, \quad \tau_{\mathrm{l,i}} = \frac{1}{2}\rho_{\mathrm{v}}u_{\mathrm{v}}^2 f - \rho_{\mathrm{v}}u_{\mathrm{v}}v_{\mathrm{v,i}}, \quad f = \frac{k}{Re_{D_{\mathrm{h}}}}. \tag{5}$$

In the friction coefficient (f), the constant, k depends on the geometric configuration. The value of 24 is used in this study for the infinite parallel-plate [11]. In addition, the Reynolds number is defined based on the hydraulic diameter, D_{h} which varies along the flow direction and sets to δ (i.e., $D_{\mathrm{h}} \approx \delta$).

The velocity of the liquid phase, u_{l} can be obtained from the mass conservation equation. The evaporative mass flow rate through the liquid–vapor interface, $\dot{m}_{\mathrm{ev}}$ is given by

$$\dot{m}_{\mathrm{ev}} = \rho_{\mathrm{l}}A_{\mathrm{l,i}}v_{\mathrm{l,i}} = \rho_{\mathrm{v}}A_{\mathrm{v,i}}v_{\mathrm{v,i}}, \tag{6}$$

where $v_{\mathrm{l,i}}$ and $v_{\mathrm{v,i}}$ are the y-directional velocities of the liquid and vapor phases, respectively, at the liquid–vapor

interface. $A_{l,i}$ and $A_{v,i}$ denote the liquid- and vapor-side areas, respectively.

Applying the mass conservation theory to the control volume, as shown in Fig. 2, we can obtain the equation

$$u_l \frac{d\delta}{dx} + \delta \frac{du_l}{dx} + v_{l,i} = 0. \tag{7}$$

The evaporative velocity, $v_{l,i}$, can be obtained using the relationship between heat flux and evaporative mass flow rate which is defined as

$$\dot{m}_{ev} = \frac{\int_x^{x+dx} q'' dx}{h_{fg}} = \frac{q'' A_w}{h_{fg}}, \tag{8}$$

where h_{fg} represents the latent heat of vaporization.

Combining Eq. (6) with Eq. (8), the evaporative velocity for the liquid phase can be calculated as

$$v_{l,i} = \frac{q'' A_w}{\rho_l A_{l,i} h_{fg}}. \tag{9}$$

Thin film region: The Navier–Stokes equation in the thin film region can be approximated by the lubrication theory. Using the boundary conditions for a shear stress at the liquid–vapor interface ($y = \delta$) and a no-slip at the liquid–solid interface ($y = 0$), the equation for the liquid pressure can be obtained as

$$\frac{dP_l}{dx} = \frac{3}{2\delta}\left(\delta - \frac{H}{2}\right)\frac{dP_v}{dx} - \frac{3\nu_l}{\delta^3}\dot{m}_l, \tag{10}$$

where $\dot{m}_l$ represents the liquid mass flow rate per unit width.

2.2. Vapor phase

Meniscus region: For the vapor phase, the following governing equations are obtained using the momentum and the mass conservation equations for streamwise direction as in the liquid phase (see Fig. 2).

$$-(\rho_v u_v^2 + P_v)\frac{d\delta}{dx} + 2\rho_v\left(\frac{H}{2} - \delta\right)u_v \frac{du_v}{dx} + \left(\frac{H}{2} - \delta\right)\frac{dP_v}{dx} = -\tau_{v,i}, \tag{11}$$

$$-u_v \frac{d\delta}{dx} + \left(\frac{H}{2} - \delta\right)\frac{du_v}{dx} - v_{v,i} = 0, \tag{12}$$

where the vapor-side shear stress at the liquid–vapor interface, $\tau_{v,i}$, has the same magnitude but the opposite direction, compared to the liquid-side shear stress which is defined in Eq. (5).

Combining Eq. (6) with Eq. (8), we can obtain the evaporative velocity of the vapor phase.

$$v_{v,i} = \frac{q'' A_w}{\rho_v A_{v,i} h_{fg}}. \tag{13}$$

Thin film region: The pressure variation of the vapor phase can be obtained using a form of the momentum equation similar to the one used for the liquid phase and the boundary conditions (i.e., shear stress at $y = \delta$ and symmetric condition at $y = H/2$):

$$\frac{dP_v}{dx} = \left\{\dot{m}_v + \frac{dP_l}{dx}\left(-\frac{\delta^2 H}{4\mu_l} + \frac{\delta^3}{2\mu_l}\right)\rho_v\right\} \Big/ A, \tag{14}$$

where $\dot{m}_v$ is the mass flow rate for the vapor per unit width and A is

$$A = -\frac{H^3}{24\nu_v} + \frac{\rho_v \delta H^2}{4\mu_l} + \frac{\delta H^2}{4\nu_v} - \frac{\rho_v H \delta^2}{\mu_l} - \frac{H\delta^2}{2\nu_v} + \frac{\delta^3}{3\nu_v} + \frac{\rho_v \delta^3}{\mu_l}. \tag{15}$$

3. Numerical analysis

The flow and heat transfer characteristics of the extended meniscus region of a micro-capillary channel are governed by the liquid film thickness, velocities and pressures for liquid and vapor phases. The governing equations in the meniscus region (i.e., Eqs. (3), (4), (7), (11) and (12)) are expressed as second-order and nonlinear ordinary differential equations. Therefore, the following inlet conditions are needed to solve them.

$$\begin{aligned} &\delta_0 = H/2.5, \quad \left.\frac{d\delta}{dx}\right|_0 = \text{specific}, \\ &u_{v,0} = 0, \quad u_{l,0} = \text{specific}, \\ &P_{v,0} = P_{v,sat}(T_{v,0}), \quad P_{l,0} = P_{v,0} - \frac{\sigma}{(H/2 - \delta_0)} - \frac{\overline{A}}{\delta_0^3}. \end{aligned} \tag{16}$$

To prevent the singularity in Eq. (3), the inlet film thickness of $\delta_0 = H/2.5$ is used. The gradient of the film thickness at the inlet is set to a large negative value. The inlet pressure of the vapor phase is set to a pressure at a saturation temperature of 383 K, and the experimental data of Khrustalev and Faghri [12] was used to obtain the inlet velocity of the liquid phase ($u_{l,0} = 0.027$ m/s). Computation starts with the meniscus region. In the meniscus region, the flow and thermal characteristics are investigated by solving the governing equation with the inlet conditions, using the 6th order Runge–Kutta method. The pressures for the liquid and vapor phases are obtained by using the finite difference method. In this calculation, the x-location where the disjoining pressure is greater than or equal to the capillary pressure is treated as the starting point of the thin film region (or junction of the meniscus and thin film regions). Thus, the values corresponding to all variables (δ, u_v, u_l, P_v, P_l) at this point are used as the inlet conditions for the thin film region. With conditions calculated and the governing equations (i.e., Eqs. (3), (10) and (14), the transport phenomena for the thin film region are examined until the value of the thin film thickness is equal to 10^{-9} m which is the value of liquid film thickness in the adsorbed region [13].

4. Results and discussion

A new mathematical formula employing different analytical approaches for the meniscus and thin film regions are presented in order to examine the transport phenomena in the extended meniscus region. Based on the developed model, the two-phase flow and thermal phenomena are investigated numerically. Water is used as the working fluid at a saturation temperature of 383 K.

4.1. Flow and thermal characteristics

The typical profile of the liquid film thickness (δ) in the extended meniscus region is shown in Fig. 3. The channel height is 150 μm, the inlet velocity of liquid phase is 0.027 m/s, and the heat flux is 1.0 MW/m^2. It can be seen from Fig. 3 that the liquid film decreases exponentially as the working fluid flows toward the adsorbed region. This profile is attributed to the fact that the evaporative mass flux due to the applied heat is much larger in the thin film than in the meniscus region.

The inset in Fig. 3 shows the enlarged film thickness near the thin film region. The dotted line is the work of Park et al. [4]. They analyzed only the thin film region. The location of $x = 0$ mm in the inset indicates $x = 3.264$ mm in the extended meniscus region (i.e., the junction of the meniscus and thin film regions). The length of the thin film region (L_{thin}) is 17.5 μm that corresponds to about 0.5% of the extended meniscus region and the liquid film thickness at the inlet of thin film region (δ_j) is estimated to be 16.2 nm. Park et al. predicted that $L_{\text{thin}} = 8.2$ μm and $\delta_j = 23.4$ nm. The discrepancy between our results and those of Park et al. may be due to the mathematical model and the boundary conditions at $\delta = \delta_j$.

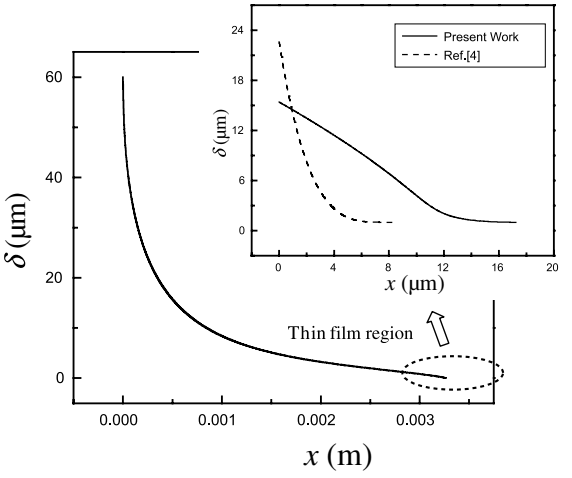

Fig. 3. Liquid film thickness for extended meniscus region and thin film region.

The flow field in the extended meniscus region occurs as a result of the pressure difference of the liquid and vapor phases as shown in Eq. (3). Fig. 4 shows the pressure drop of the liquid and vapor phases along the flow direction. Both the liquid and vapor pressures decrease as the fluid flows toward the adsorbed region. This indicates that the liquid and vapor phases flow in the same direction. This result is different from that obtained by Longtin et al. [6] in which the liquid and vapor phases flow in the opposite direction. The figure also shows that the liquid pressure drop is several hundred times greater than the vapor pressure drop. Therefore, it can be concluded that the shear stress at the liquid–vapor interface is mainly due to the liquid pressure drop and the flow characteristic in the evaporator is strongly influenced by the liquid rather than by the vapor pressure.

Table 1 shows the local heat transfer coefficients for several x-locations. The local heat transfer coefficient (h) is defined as

$$h(x) \approx \frac{k_l}{\delta(x)}. \tag{17}$$

The local heat transfer coefficient in the meniscus region is small, while that in the thin film region is extremely large. The abrupt increase of $h(x)$ in the thin film region is due to the reduced thermal resistance by the thinner liquid film thickness. The average heat transfer coefficients for the meniscus and thin film regions are 31.4 and 14,293, respectively. The heat transfer rate, however, is

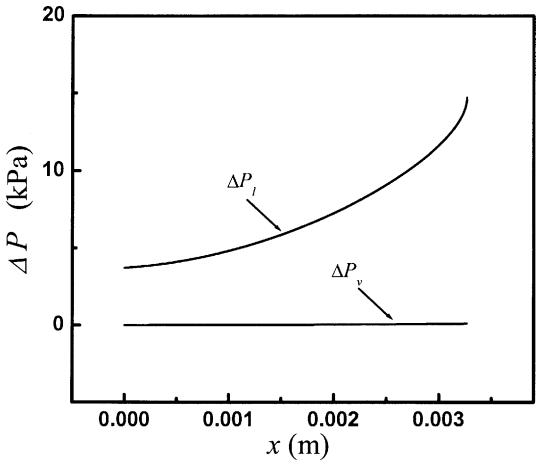

Fig. 4. Pressure drop of the liquid and vapor phases.

Table 1
Local heat transfer coefficients for various locations

x (mm)	1	2	3	3.2641[a]	3.2665
h (W/m^2 K)	7.1	18.2	70.6	2673.7	57944.0

[a] Starting point of the thin film region.

larger for the meniscus than for the thin film region because of the very short length of the thin film region.

4.2. Effects of heat flux and inlet liquid velocity

Fig. 5 represents the predicted liquid and vapor velocities under the various heat flux conditions. For a constant heat flux, the liquid velocity gradually increases and has a maximum value at the location of 40% of the extended meniscus region. Thereafter, the liquid velocity decreases and finally approaches zero. The profile of the liquid velocity is similar for all heat flux conditions.

The maximum liquid velocities and their locations are listed in Table 2. The variation of the heat flux has a negligible effect on the maximum liquid velocities. The location of the maximum velocity shifts toward the inlet of the extended meniscus region as the heat flux increases.

Fig. 5(b) presents the effect of the heat flux on the vapor velocity. The vapor velocity increases linearly along the flow direction and increases sharply near the thin film region. It should be noted that the evaporative mass flux in the thin film region is dramatically increased due to high heat transfer, as shown in Table 1. The maximum vapor velocity does not change even though the heat flux increases. Comparing Fig. 5(a) with Fig. 5(b), the vapor velocity is much larger than the liquid velocity for the same x-location and a constant heat flux, as expected. Notice that the vapor velocity is about one thousand times as fast as the liquid velocity under a given heat flux.

Table 2
Maximum liquid velocities and their locations with heat flux

	Heat flux (q'', MW/m^2)		
	0.8	1.0	1.2
$u_{l,max}$ (mm/s)	31.65	31.98	32.48
Corresponding x-location (mm)	1.62	1.24	1.13

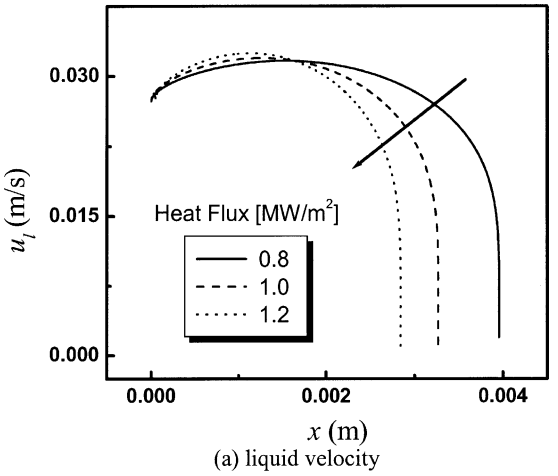

(a) liquid velocity

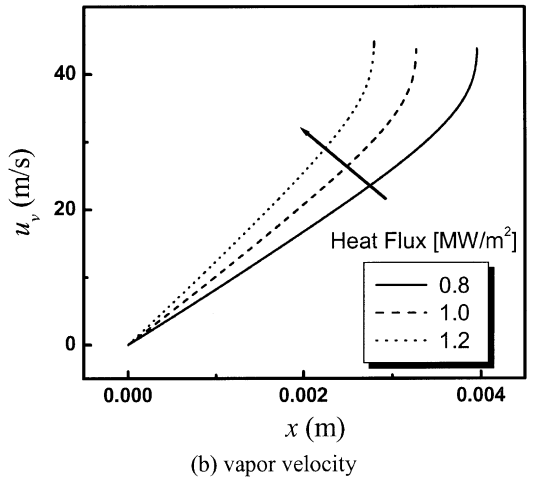

(b) vapor velocity

Fig. 5. Liquid and vapor velocities with heat flux.

Fig. 6 shows the profile of the liquid film thickness for various inlet liquid velocities. The film thickness and length of the extended meniscus region decrease with increasing inlet liquid velocity. This is mainly due to the increased pressure difference between the liquid and vapor phases with increasing inlet liquid velocity. However, the influence of the inlet liquid velocity on the profile of the film thickness is less significant.

4.3. Dry-out point

The most important factor in designing the micro-evaporator is to predict the location where the dry-out phenomenon occurs (i.e., accurate determination of the length of the extended meniscus region).

Another interesting result predicted from the present model is shown in Fig. 7, which gives the length of the

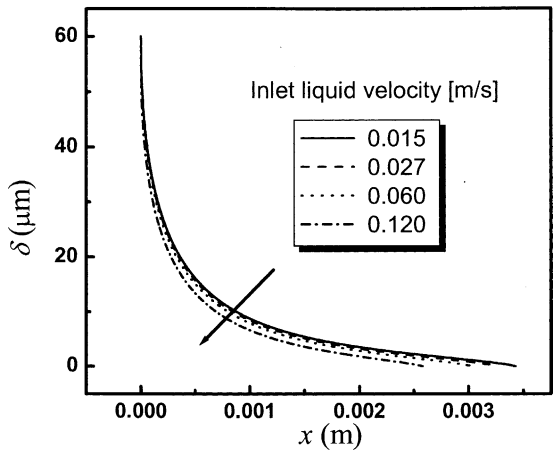

Fig. 6. Liquid film thickness with inlet liquid velocity.

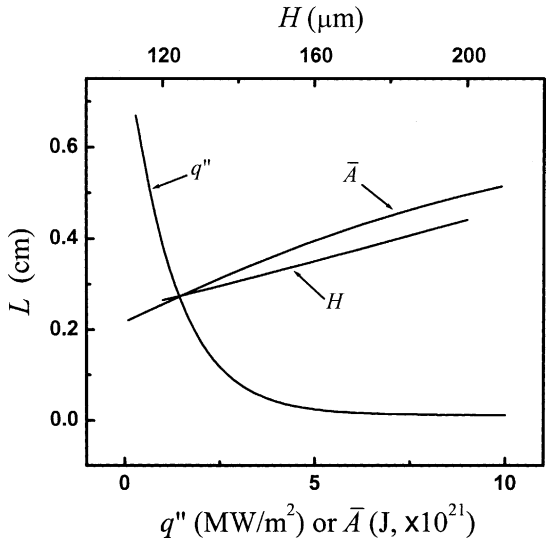

Fig. 7. Effect of heat flux, channel height, and dispersion constant on the length of the extended meniscus region.

extended meniscus region for various heat fluxes (q''), channel heights (H), and dispersion constants ($\overline{A}$). In the figure, the baseline conditions for them are $H = 150$ μm, $q'' = 1$ MW/m^2, and $A = 2.87 \times 10^{-21}$ J. The length of the extended meniscus region decreases exponentially with increasing heat flux. This is due to the decreased liquid film thickness caused by the increased evaporative mass flux at the liquid–vapor interface as the heat flux increases. For $q'' < 5$ MW/m^2, L decreases dramatically, but for $q'' > 5$ MW/m^2, L does not change. This implies that the variation of the heat flux has a negligible effect on the length of the extended meniscus region if the heat flux is greater than 5 MW/m^2. In addition, when $q'' > 5$ MW/m^2, the value of L is about 0.2 mm.

The liquid film thickness increases with channel height because of the attenuated pressure gradient of liquid phase. The thicker film thickness causes the evaporative mass flux at the liquid–vapor interface to decrease and L increases linearly.

The length of the extended meniscus region increases linearly with the dispersion constant. The reason for this is that for a larger dispersion constant, the extended meniscus region is extended farther down the channel because the attractive force strongly acts on the region between the liquid and the solid wall. Therefore, it can be concluded that the surface treatment plays an important role in designing the micro-evaporator because the dispersion constant is strongly related to the surface roughness.

5. Conclusions

In this study, a mathematical model describing the two-phase flow and thermal characteristics of the extended meniscus region in a micro-capillary channel was successfully developed. Based on the developed model, fundamental transport phenomena were investigated and the effects of various parameters on the flow and heat transfer performance were also discussed.

The results showed that the profile of the liquid film thickness decreased exponentially and the vapor and liquid phases flow in a parallel-flow manner. The local heat transfer coefficient has a very large value in the thin film region. The heat transfer rate, however, is larger for the meniscus than for the thin film region. The influence of inlet liquid velocity on the profile of the liquid film thickness was less significant. The maximum liquid velocity occurred at approximately 40% of the extended meniscus region and the variation of the heat flux had a negligible effect on it. With increasing heat flux, the length of the extended meniscus region decreased exponentially. However, the length of the extended meniscus region linearly increased with the dispersion constant and the channel height.

Acknowledgements

This research was supported by The Center of Innovative Design Optimization Technology (iDOT), Korea Science and Engineering Foundation.

References

[1] B.V. Derjaguin, S.V. Nerpin, N.V. Churaev, Effect of film transfer upon evaporating liquids from capillaries, RILEM Bull. 29 (1) (1965) 93–98.
[2] X. Xu, V.P. Carey, Film evaporation from a micro-grooved surface—an approximate heat transfer model and its comparison with experimental data, AIAA J. Thermo-Phys. Heat Transfer 4 (4) (1990) 512–520.
[3] J.M. Ha, G.P. Peterson, The interline heat transfer of evaporating thin film along a micro grooved surface, ASME J. Heat Transfer 118 (1996) 747–755.
[4] K. Park, K.J. Noh, K.S. Lee, Transport phenomena in the thin film region of a micro-channel, Int. J. Heat Mass Transfer 46 (2003) 2381–2388.
[5] S. DasGupta, J.A. Schonberg, P.C. Wayner Jr., Investigation of an evaporating extended meniscus based on the augmented Young–Laplace equation, ASME J. Heat Transfer 115 (1993) 201–210.
[6] J.P. Longtin, B. Badran, F.M. Gerner, A one-dimensional model of a micro heat pipe during steady-state operation, ASME J. Heat Transfer 116 (1994) 709–715.
[7] V. Sartre, M. Zaghdoudi, M. Lallemand, Effect of interfacial phenomena on evaporative heat transfer in micro heat pipes, Int. J. Therm. Sci. 39 (2000) 498–504.
[8] Y.P. Peles, S. Haber, A steady state, one dimensional model for boiling two phase flow in triangular micro-channel, Int. J. Multiphase Flow 26 (2000) 1095–1115.

[9] W. Qu, T. Ma, J. Miao, J. Wang, Effects of radius and heat transfer on the profile of evaporating thin liquid film and meniscus in capillary tubes, Int. J. Heat Mass Transfer 45 (2002) 1879–1887.
[10] F. Blangetti, M.K. Naushahi, Influence of mass transfer on the momentum transfer in condensation and evaporation phenomena, Int. J. Heat Mass Transfer 23 (1980) 1694–1695.
[11] A. Bejan, Convection Heat Transfer, second ed., John Wiley & Sons, Inc., 1995, pp. 102–104.
[12] D. Khrustalev, A. Faghri, Thick-film phenomenon in high-heat-flux evaporation from cylindrical pores, ASME J. Heat Transfer 119 (1997) 272–278.
[13] J.H. Lay, V.K. Dhir, Shape of a vapor stem during nucleate boiling of saturated liquids, ASME J. Heat Transfer 117 (1995) 394–401.